FIBER TOW DEFORMATIONS DURING LAYUP OF STEERED PATHS USING AUTOMATED FIBER PLACEMENT PROCESS

Roudy Wehbe, Brian Tatting, Zafer Gürdal, Ramy Harik

McNAIR Center for Aerospace Innovation and Research, Department of Mechanical Engineering, College of Engineering and Computing, University of South Carolina
1000 Catawba St., Columbia, SC, 29201, USA

ABSTRACT

Automated Fiber Placement (AFP) is a manufacturing process used to fabricate composite structures for aerospace applications. For simple conventional laminated plate structures manufactured using the AFP process, fibers are laid at constant angles (0°, 90°, ±45°) in straight paths. However, to manufacture complex shell structures or variable stiffness plates, the straight fiber tows must deform to adhere to the curved paths. In this paper, those deformations are classified as strain deformations (tensile, compressive, shear), large in-plane deformations (waviness and bunching), and out-of-plane deformations (wrinkling and folding). The aim of this paper is to understand which of these deformation mechanisms is predominant during the manufacturing process. To do so, the carbon fiber tow is modeled as multiple fiber bundles placed on a stiff elastic foundation within a constrained curved path. The governing nonlinear differential equations are derived based on minimizing the total energy of the system, and the final shape of the deformed tow is obtained by solving the system numerically. Mainly, compressive strains, fiber waviness, and/or wrinkling are the main deformation modes on the compressive side of the tow, whereas tensile strain, fiber bunching, and/or tow folding occur on the tensile side. The importance of the material properties, radius of curvature, stiffness of the foundation and other process parameters on the final shape of the deformed tow is also discussed.

1. INTRODUCTION

The usage of Automated Fiber placement (AFP) especially in the aerospace industry is gaining advantage over hand layup due to improvements in productivity, and over automated tape laying due to the possibility of manufacturing complex shapes. Traditionally, fibers are laid at constant angles in straight paths over flat tools, however, manufacturing complex shell structures using AFP machines requires steering fibers possibly over doubly curved tools even for constant-angles paths [1]. In addition, having the ability to steer fiber tows on flat surfaces, fiber placement machines can thus increase the design space of composite structures by allowing the manufacture of variable stiffness panels [2]. However during the manufacturing process, several defects may arise [3] for several reasons such as material variability, geometry, machine parameters or others, hence possibly reducing the quality of the produced part. Concerning tow steering using AFP, the process is limited to defects that occur due to the mismatch in length between the straight tow and the curved tow-path on the tool such as wrinkling and folding [4]. To absorb this difference in length, several mechanisms are proposed in the literature ([5],[6]), and classified as follows: (a) strain deformations such as tensile, compressive, and shear which are uniform along the length,

SAMPE Conference Proceedings. Charlotte, NC, May 20-23, 2019. Society for the Advancement of Material and Process Engineering – North America.

(b) localized in-plane deformations such as in-plane waviness and tow straightening/bunching, and (c) localized out-of-plane deformations such as wrinkling and folding (see Figure 2 and Figure 1).

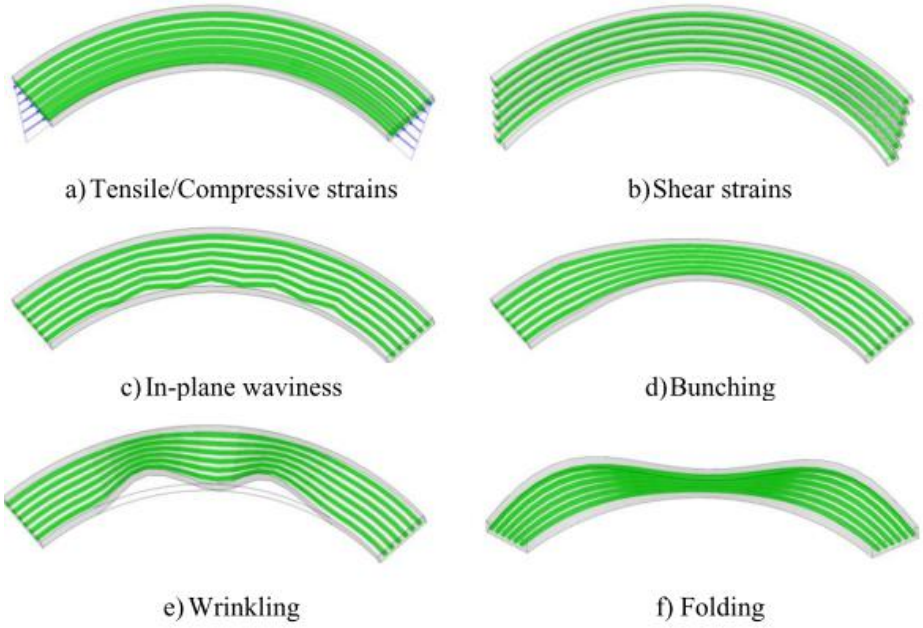

Figure 1. Deformation mechanisms for differential length absorption [5]

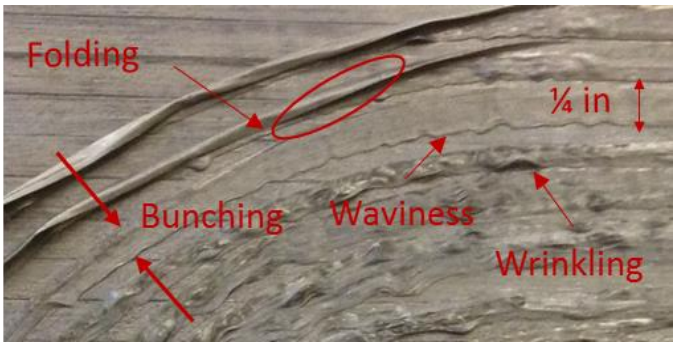

Figure 2. Tow deformations due to excessive steering (Courtesy of McNair Center, University of South Carolina) [6]

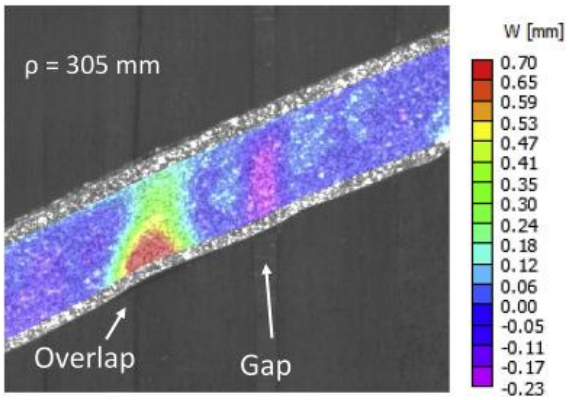

Figure 3. Effect of substrate defect on the out-of-plane deformations of a steered tow [7]

Experimental measurements of these deformations can be accomplished using stereo digital image correlation [7], and the results show a strong interaction between the steered tow and the tool substrate (Figure 3). Regarding the modeling efforts of these deformations, tow wrinkling is modeled in the literature as a plate resting on an elastic foundation for the case of thermoset [8] and dry fiber [9] tows. The limitation of these models is their inability to capture defects that occur on the tensile side of the tow such as folding, their inability to capture in-plane deformations, and it is difficult to extend these models for the case of tows laid on general surfaces. Another model to predict wrinkling that extends to general surfaces is presented in the literature ([5], [10]) based

on the geometry of the tow-path. As for the case of modeling in-plane deformations due to steering, fiber waviness is investigated as a possible mechanism on the compressive edge of the tow [11]. However, the deformed shape was assumed to be sinusoidal, and the corresponding amplitude and wavelength are determined statistically from experiments. Another model that captures both the tensile and compressive in-plane deformations such as waviness and bunching is presented by the authors [6]. This paper is an extension to the previous model to include the out-of-plane deformations of the tow during the AFP process.

In this paper, the carbon fiber tow used in the AFP process is modeled as several fiber bundles laying on a stiff foundation. The total energy of the system is derived for the case of small strains and large rotations, allowing the bundles to deform in space while being restricted by the foundation stiffness and the boundary conditions enforced by the roller. The detailed derivations of the equilibrium equations and the numerical solution approach to solve them are presented in Section 2. The results for a tow placed on a constant curvature path are shown in Section 3 along with an investigation of the effect of the stiff foundation and the tow length. Finally, conclusion, recommendations and future work are discussed in Section 4.

2. GOVERNING EQUATIONS

In this section, the derivations of the equilibrium equations for a single bundle deforming in space are shown first. Then a numerical solution algorithm is presented showing how the obtained governing equations are solved.

2.1 Derivation of the Equilibrium Equations

During the AFP process, the machine head by the means of the roller forces the tow to adhere to a substrate following a prescribed path. Hence, the problem here is formulated in a way that the boundary of the tow has to satisfy a specific displacement field imposed by the roller due to steering. The thin tow is considered as several fiber bundles laying on a stiff foundation. A representation of a single bundle deformed in 2D is shown in Figure 4. Here, the in-plane deformations of the tow are induced by the end-forces f_x and f_y enforced by the roller at a specific endpoint (x_L, y_L) and at a prescribed rotation γ_L. These deformations are restricted by the stiffness of the foundation in the x and y-directions k_x and k_y representing the adhesion of the tow to the substrate [6]. For the case where the fiber bundle is allowed to deform in the out-of-plane direction, an additional force f_z is required at the endpoint, and the foundation's resistance to this deformation is represented through the stiffness term k_z. The relationship between the out-of-plane rotation angle β, the in-plane rotation γ and the corresponding arc-length and strain can be visualized in Figure 5. The total energy Π of the system can be expressed as:

$$\Pi = U - W + K\,, \qquad [1]$$

where U is the elastic strain energy, K is the energy stored in the elastic foundation, and W is the work generated by the applied forces necessary to satisfy the boundary conditions.

A simplification of the strain energy term for the in-plane case is presented in [6] where small strains and large rotations are taken into considerations for the fiber bundle. It is also assumed that the tow is highly anisotropic: the stiffness in the fiber direction is orders of magnitudes larger than the transverse stiffness and shear since these properties are mainly governed by the uncured resin.

Hence, the elastic strain energy will only include terms for related to the longitudinal stiffness, as well as the fiber extension $l'(s)$, the in-plane curvature $\gamma'(s)$, and the out-of-plane curvature $\beta'(s)$:

$$U = \frac{1}{2}\int_0^L E_{11}\left(w_b H l' + I_\gamma \gamma'^2 + I_\beta \beta'^2\right) ds, \quad [2]$$

where I_γ and I_β the moments of inertia corresponding to the in-plane bending and out-of-plane bending respectively, w_b is the width of a single bundle, and E_{11} is the stiffness in the longitudinal direction. For the case where the tow bundle has a rectangular cross section and if its shape does not change along the length, I_γ and I_β can be expressed in terms of the bundle width w and the thickness H as:

$$I_\gamma = \frac{1}{12} H\, w_b^3, \qquad I_\beta = \frac{1}{12} w_b\, H^3 \quad [3]$$

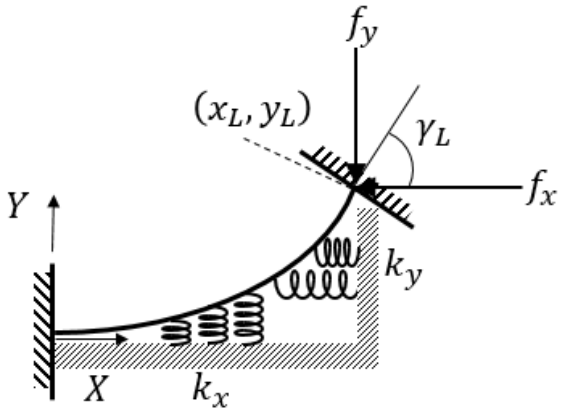

Figure 4. A 2D representation of a fiber bundle during AFP [6]

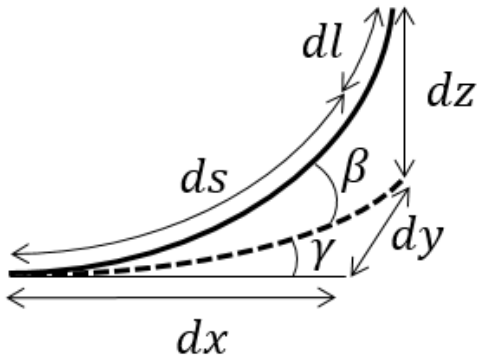

Figure 5. Strain rotation relationship in 3D

The total work W generated by the applied forces $\boldsymbol{F} = \{f_x, f_y, f_z\}$ can be expressed as:

$$W = \boldsymbol{F} \cdot \boldsymbol{\Delta}, \quad [4]$$

with $\boldsymbol{\Delta} = \{(x_L - x_0) - L, (y_L - y_0) - 0, (z_L - z_0) - 0\}$ being the total displacement vector. The relationship between differential lines in the x, y and z-directions (dx, dy and dz), strain, arc-length, and rotations is shown in Figure 5, and can be expressed as:

$$dx = (ds + dl)\cos\gamma\cos\beta = (1 + l')\cos\gamma\cos\beta\, ds, \quad [5]$$

$$dy = (ds + dl)\sin\gamma\cos\beta = (1 + l')\sin\gamma\cos\beta\, ds, \quad [6]$$

$$dz = (ds + dl)\sin\beta = (1 + l')\sin\beta\, ds. \quad [7]$$

Integrating both sides of equations [5]-[7] between 0 and the bundle length L, and inserting them back into equation [4], the expression of the total work W can be generated as:

$$W = f_x\left[\int_0^L (1 + l')\cos\gamma\cos\beta\ ds - L\right] + f_y\int_0^L (1 + l')\sin\gamma\cos\beta\ ds + f_z\int_0^L (1 + l')\sin\beta\, ds \quad [8]$$

Lastly, the energy term resulting from the elastic foundation can be expressed as:

$$K = \frac{1}{2}\int_0^L k_x\, u^2(s)\, ds + \frac{1}{2}\int_0^L k_y\, v^2(s)\, ds + \frac{1}{2}\int_0^L k_z\, w^2(s)\, ds\,, \qquad [9]$$

where, k_x, k_y, k_z represents the stiffness of the foundation in the x, y, and z-directions respectively, and $u(s), v(s), w(s)$ are the displacements in these directions as well.

The final expression of the total energy can be obtained by inserting the resulting expressions of the strain energy (equation [2]), work (equation [8]), and stored energy (equation [9]) into the total energy equation [1] Therefore, the expression of the total energy contains 6 unknown functions $\gamma(s), \beta(s), l(s), x(s), y(s)$ and $z(s)$, and 3 unknown constants f_x, f_y and f_z. Note that $x(s), y(s)$ and $z(s)$ can be expressed in terms of $\gamma(s), \beta(s)$ and $l(s)$ by integrating equations [5]-[7], hence, the functional Π can be expressed in terms of the first three functions only as:

$$\Pi\big(\gamma(s), l(s)\big) = \int_0^L \mathcal{F}\big(s, \gamma(s), \gamma'(s), \beta(s), \beta'(s), l'(s)\big)\, ds \qquad [10]$$

Using Euler-Lagrange principle to minimize the total energy Π, the following set of partial differential equations has to be satisfied:

$$\begin{cases} \dfrac{d}{ds}\left(\dfrac{\partial \Pi}{\partial \gamma'}\right) - \dfrac{\partial \Pi}{\partial \gamma} = 0 \\ \dfrac{d}{ds}\left(\dfrac{\partial \Pi}{\partial \beta'}\right) - \dfrac{\partial \Pi}{\partial \beta} = 0 \\ \dfrac{d}{ds}\left(\dfrac{\partial \Pi}{\partial l'}\right) - \dfrac{\partial \Pi}{\partial l} = 0 \end{cases} \qquad [11]$$

By evaluating the partial derivatives of equation [11] the governing equations can be obtained as:

$$\begin{cases} E_{11} I_\gamma\, \gamma'' - f_x \sin\gamma\cos\beta + f_y \cos\gamma\cos\beta + k_x uy - k_y vx = 0 \\ E_{11} I_\beta \beta'' - f_x \cos\gamma\sin\beta - f_y \sin\gamma\sin\beta + f_z \cos\beta + k_x u\xi + k_y v\psi - k_z w\zeta = 0 \\ E_{11} A l' = \big(F + f_x \cos\gamma\cos\beta + f_y \sin\gamma\cos\beta + f_z \sin\beta - k_x ux - k_y vy - k_z wz\big) \\ x' = (1 + l')\cos\gamma\cos\beta \\ y' = (1 + l')\sin\gamma\cos\beta \\ z' = (1 + l')\sin\beta \\ \xi' = (1 + l')\cos\gamma\sin\beta \\ \psi' = (1 + l')\sin\gamma\sin\beta \\ \zeta' = (1 + l')\cos\beta \end{cases} \qquad [12]$$

Note that in the above system of equations, the first three equations correspond to the equilibrium equations (in-plane bending, out-of-plane bending, and fiber extension respectively). The next three equations relate the coordinates to the fiber's extension and rotations similarly to equations [5]-[7]. The last three equations in terms of ξ', ψ', and ζ' are introduced as intermediate variables to avoid having their integral form in the out-of-plane bending equation. Note that all 9 equations shown above have to be solved simultaneously as a system of equations.

2.2 Numerical Solution Approach

The system of equations shown in [12] is a system of nonlinear differential equations, containing 2nd order derivatives for γ and β, and 1st order derivatives for $l, x, y, z, \xi, \psi,$ and ζ. Hence, eleven boundary conditions are needed for these functions. The starting point of the path can provide nine of them:

$$\text{At s} = 0\text{: } \gamma(0) = \gamma_0, \beta(0) = \beta_0, l(0) = l_0, x(0) = x_0, y(0) = y_0, z(0) = z_0\ , \quad \xi(0) = \psi(0) = \zeta(0) = 0. \tag{13}$$

Note that the intermediate variables are chosen to be zero at the start point for numerical convenience. The remaining two boundary conditions are obtained at the endpoint:

$$\text{At s} = \text{L: } \gamma(L) = \gamma_L, \beta(L) = \beta_L. \tag{14}$$

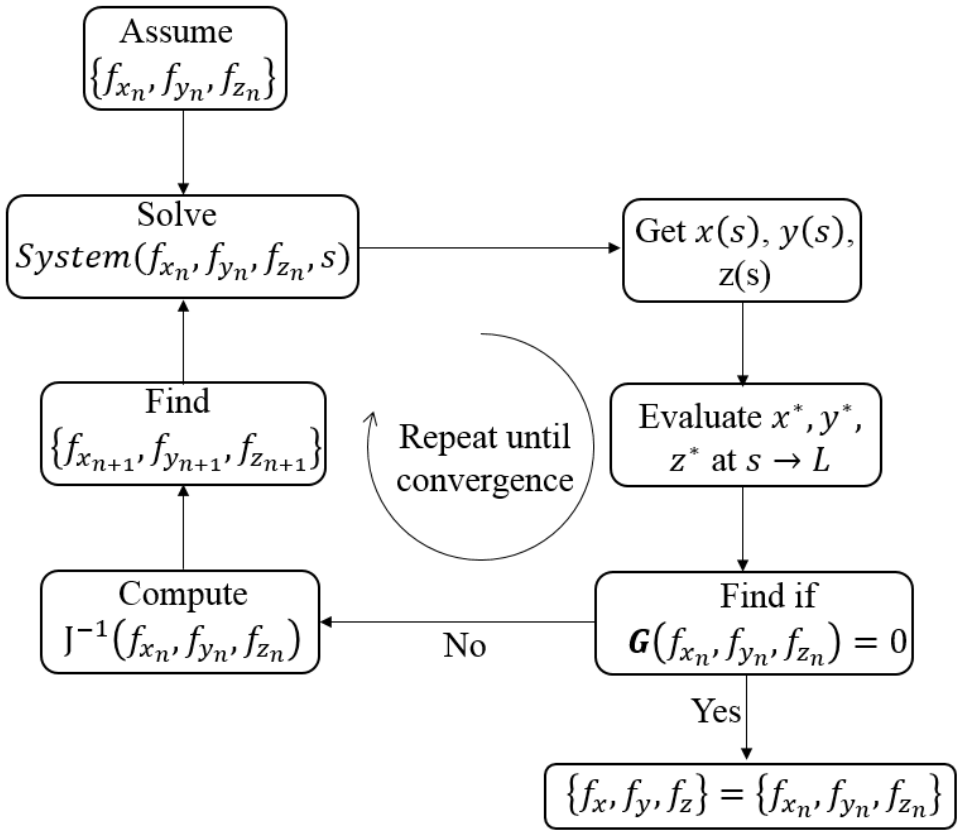

Figure 6. Iterative approach to obtain the unknown forces

In addition to the unknown functions, the system of equations shown in [12] contains three unknown forces f_x, f_y and f_z. These forces have to satisfy three remaining boundary conditions x_L, y_L and z_L; the coordinates of the endpoint of the fiber bundle enforced by the roller at s = L. To accomplish that, an iterative approach is implemented as shown in Figure 6. Here, $System(f_x, f_y, f_z, s)$ refer to the system of equations [12] where the forces are unknown. First, an initial value for the forces is assumed. A good starting point can be assumed as $f_{x_0} = f_{y_0} = f_{z_0} = 0$. Then, the system in [12] can be solved for these assumed values, and the functions

$x(s), y(s)$ and $z(s)$ can be obtained. To ensure the boundary conditions are fulfilled, the following vector function providing three additional equations must be satisfied:

$$\boldsymbol{G}(f_x, f_y, f_z) = \begin{Bmatrix} x^*(f_x, f_y, f_z) - x_L \\ y^*(f_x, f_y, f_z) - y_L \\ z^*(f_x, f_y, f_z) - z_L \end{Bmatrix} = \mathbf{0}\,, \qquad [15]$$

where $x^*, y*$ and z^* are the values of $x(s), y(s)$ and $z(s)$ evaluated at s = L. The Newton-Raphson method is applied to the system of equations in [15] iteratively to determine the forces f_x, f_y and f_z such that:

$$\begin{Bmatrix} f_{x_{n+1}} \\ f_{y_{n+1}} \\ f_{z_{n+1}} \end{Bmatrix} = \begin{Bmatrix} f_{x_n} \\ f_{y_n} \\ f_{z_n} \end{Bmatrix} - c\, J^{-1}\left(f_{x_n}, f_{y_n}, f_{z_n}\right)\, \boldsymbol{G}\left(f_{x_n}, f_{y_n}, f_{z_n}\right), \qquad [16]$$

where $J\left(f_{x_n}, f_{y_n}, f_{z_n}\right)$ is the Jacobian matrix for the vector function $\boldsymbol{G}\left(f_{x_n}, f_{y_n}, f_{z_n}\right)$:

$$J = \left[\frac{\partial \boldsymbol{G}\left(f_{x_n}, f_{y_n}, f_{z_n}\right)}{\partial f_x} \quad \frac{\partial \boldsymbol{G}\left(f_{x_n}, f_{y_n}, f_{z_n}\right)}{\partial f_y} \quad \frac{\partial \boldsymbol{G}\left(f_{x_n}, f_{y_n}, f_{z_n}\right)}{\partial f_y}\right]. \qquad [17]$$

Note that the vector function $\boldsymbol{G}(f_x, f_y, f_z)$ requires solving the system in [12] numerically then evaluating the numerical values of x^*, y^* and z^* at $s = L$. Therefore, the partial derivatives in the Jacobian matrix in [17] cannot be evaluated analytically and a numerical method must be used, such as a finite difference technique.

3. RESULTS

In this section, the developed governing equations and numerical solution approach are implemented for the specific case of a tow placed on a flat surface and following a circular path. The corresponding end-point boundary conditions are first presented. Then, the results are shown for a combined tensile and compressive region within the tow. The effect of the length of the tow as well as the foundation stiffness are also investigated.

3.1 Boundary Conditions

A steered tow-path at a constant curvature is considered for investigation. A possible arc-length parametrization for a constant curvature path (circular arc) is [6]:

$$\boldsymbol{C}(s) = \{x(s), y(s), z(s)\} = \begin{cases} \rho\ \sin(s/\rho) \\ \rho[1 - \cos(s/\rho)]\,, \\ 0 \end{cases} \quad 0 \le s \le L, \qquad [18]$$

where ρ is the constant radius of curvature. If we consider that $\boldsymbol{C}(s)$ is the centerline of the tow-path, then the parallel edges of the tow-path can be found by taking the parallel curves to $\boldsymbol{C}(s)$ which can be expressed as follows [9]:

$$\boldsymbol{C_p}(s) = \{x_p(s), y_p(s), z_p(s)\} = \begin{cases} (d+\rho)\ \sin(s/\rho) \\ \rho - (d+\rho)\cos(s/\rho)]\,, \\ 0 \end{cases} \quad 0 \le s \le L, \qquad [19]$$

where d can be either a positive or a negative distance. For the case where d is positive, the parallel edge obtained by equation [19] corresponds to a path $\boldsymbol{C_p}(s)$ longer than the reference path $\boldsymbol{C}(s)$,

or in other words, the tensile side of the tow. Whereas a negative value of d corresponds to the compressive edge of the tow. The enforced boundary condition at the endpoint can be obtained using the following:

$$x_L = x_p(L), y_L = y_p(L) + d, z_L = 0, \gamma_L = \frac{L}{\rho}, \beta_L = 0. \quad [20]$$

Note that for numerical convenience, the parallel paths are shifted along the y-axis by a distance d, so that the y-coordinate of the start point corresponds to zero. Concerning the start point, all boundary conditions for the coordinates, rotations, strain, and intermediate variables are chosen to be zero. The out-of-plane rotation as well as the z coordinate are forced to be zero at the start and the end of the fiber bundle, due to the roller motion and similar to the clamped boundary conditions.

3.2 Results for a combined tension/compression region

In a first step to analyze the out-of-plane, a worst-case scenario is considered where there is no adhesion ($k_x = k_y = k_z = 0$). Other relevant parameters such as radius of curvature, tow thickness, width and modulus for an uncured thermoset pre-impregnated tow are shown in Table *1*. The shape of the deformed fibers in the compressive side of the tow as well as the tensile side are shown in Figure 7 for a length of 4 cm. For this case, half the tow width is assumed under compression, and the other half under tension. Five bundles are chosen here for analysis where two of them are laying in the region under compression, two in the region under tension, and one coinciding with the neutral axis. The deformed curve representing the centroid of each fiber bundle is shown in Figure 7 using a dotted line, whereas the tensile and compressive edges are shown using solid lines.

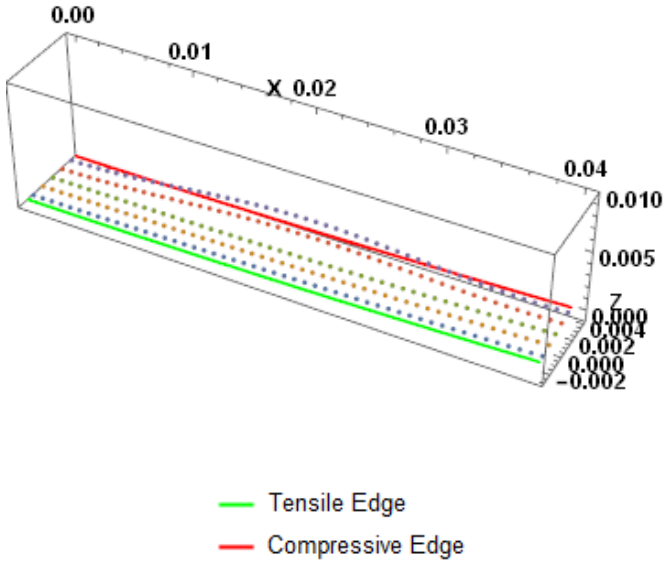

Figure 7: Deformed fiber bundles in 3D under combined loading

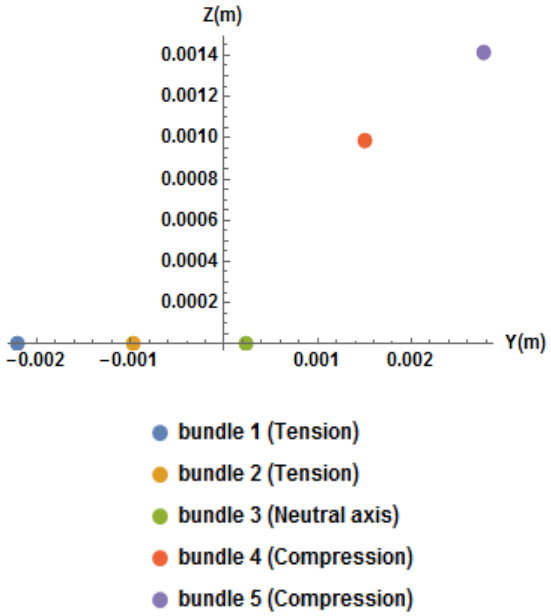

Figure 8: Maximum z-displacement of the fiber bundles at L/2

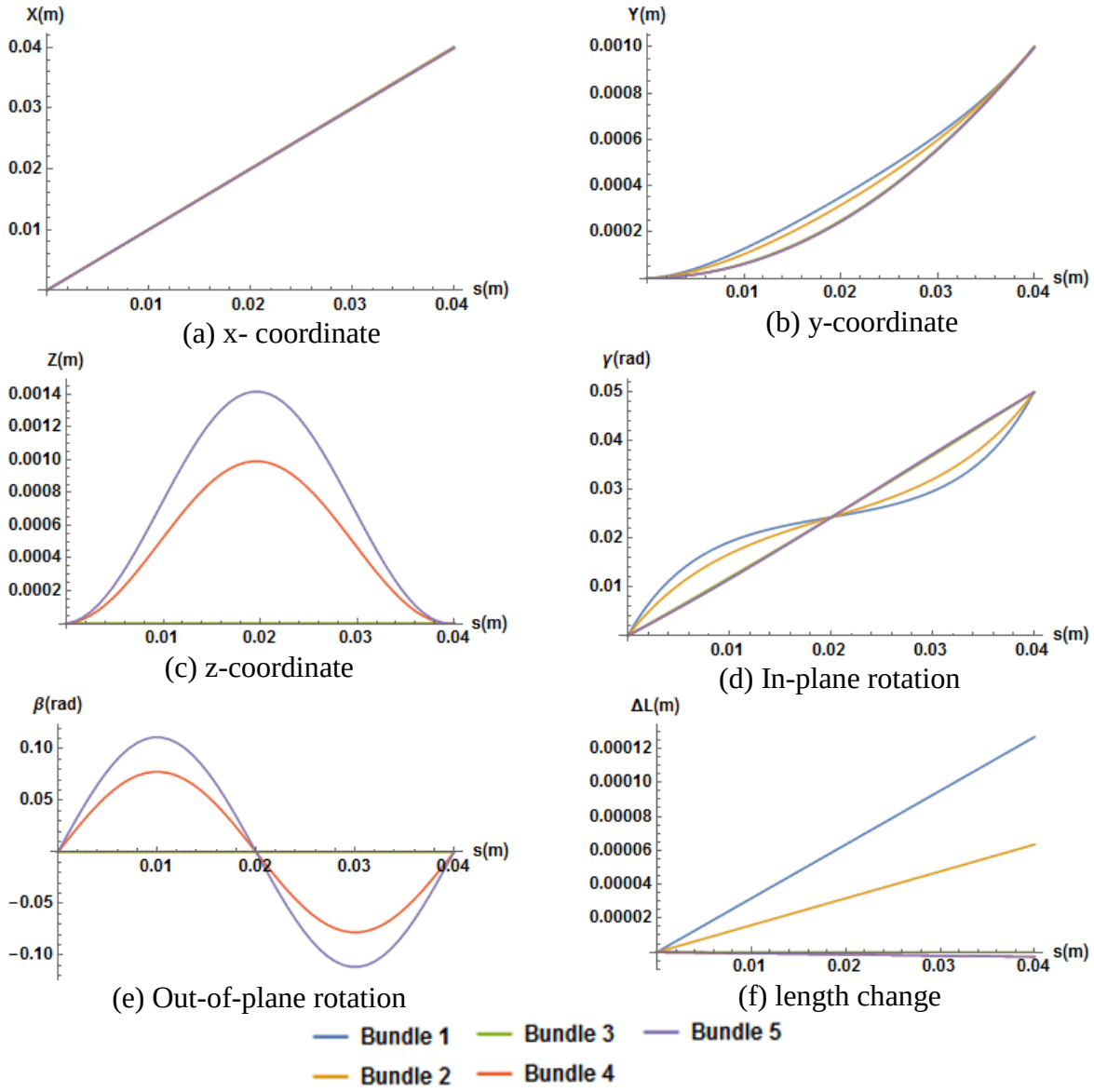

Figure 9: Solution of equation [12] for 5 bundles under combined loading

Table 1: Material property and geometry of the tow deforming out-of-plane

E_{11}	H	w	ρ	$k_x = k_y = k_z$	L
130 GPa	0.184 mm	6.35 mm	0.8 m	0	4 cm

A first look at the deformed shape of the tow in Figure 7 shows that the fiber bundles on the compressive edge of the tow have deformed in the out-pf-plane direction to form a wrinkle. The remaining fiber bundles laying on the neutral axis and in the tensile region have deformed in-plane. A detailed view of tow cross-section taken at half-length showing the maximum displacement in

the z-direction is shown in Figure 8. This confirms that only the bundles under compression are deforming in the out-of-plane direction. Details of the results of the governing equation [12] for the five bundles are shown in Figure 9. Bundles 4 and 5 in the compressive region deform out-of-plane as shown in the z-coordinate plot and the out-of-plane rotation angle β. Bundle 3 coinciding with the neutral axis remains in-plane and parallel to the path, whereas the bundles under tension deformed in-plane in the fiber bunching/straightening mode. This is reflected in the plot of the y-coordinate as well as in the in-plane rotation angle γ. Lastly, the axial strain represented in the length change plot shows that the fiber bundles on the tensile side have extended significantly to absorb the length difference, however, the axial strain for the bundles under compression is significantly smaller, indicating that most of the length difference is compensated for by the out-of-plane deformation.

3.3 Effect of the Length

In this section, the effect of the length of the fiber bundles is investigated for five bundles placed under compression. The material properties and tow geometry are the same as the one used in the above section (see Table 1). Three different bundle lengths (1, 2, and 4 cm) are investigated, and the results showing the deformed shape of the tow bundles are presented in Figure 10. At a small length of 1 cm, the fiber bundle remains in-plane, and the differential length is absorbed by means of compressive strains. However, as the length increases, the fiber bundles closest to the compressive edge starts to deform in the z-direction as shown for the case of L = 2 cm, except the fiber bundle closest to the neutral axis which remains in-plane. This is due to the fact that the differential length close to the neutral is small and increases as the fiber are placed further away from the neutral axis. At a significantly larger length, all fiber bundles under compression buckle in the out-of-plane direction to form a wrinkle.

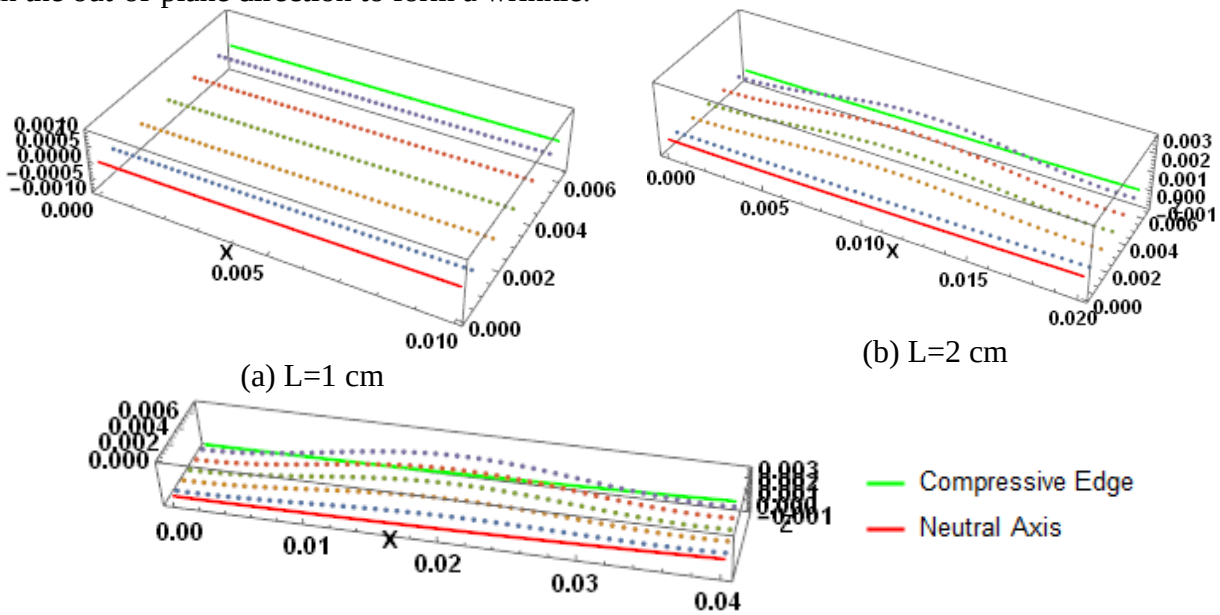

(a) L=1 cm

(b) L=2 cm

(c) L = 4 cm

Figure 10: Effect of the length on the out-of-plane deformation of bundles under compression

3.4 Effect of the foundation stiffness

In this set of results the effect of the stiffness foundation on the deformed shape of the fiber bundles is investigated. A reasonable assumption can be made where the foundation is isotropic having similar values in the x , y and z-directions. Other material properties and tow geometry are shown in Table *2*. In this case, the length of the tow section, as well as the steering radius are kept constant, whereas the value of the foundation stiffness is varied between 0 and 10^8 N/m^2. The tow is assumed to be under compression, where five equal separate regions are considered for the analysis.

To quantify the effect of the foundation's stiffness on the deformation of the fiber bundles, we focus on the displacement in the z- direction. This corresponds to the z-coordinate, since it is assumed that the fiber bundles are placed on a flat surface. The results for the five fiber bundles are shown in Figure 11 for different values of the foundation's stiffness (logarithmic scale). Large values of k ($k > 10^6\ N/m^2$) result in zero displacement in the z- direction: this means that the foundation is stiff enough to hold the fibers in their intended location, and the layup is wrinkle free. For small values of k ($k < 10^5\ N/m^2$), the displacement in the z- direction is constant and does not change from the value of $k = 0$. This indicates that the foundation is very weak and unable to resist the out-of-plane deformation.

Table 2: Material property and geometry of the tow

E_{11}	H	w	L	ρ
130 GPa	0.184 mm	6.35 mm	2 cm	0.8 m

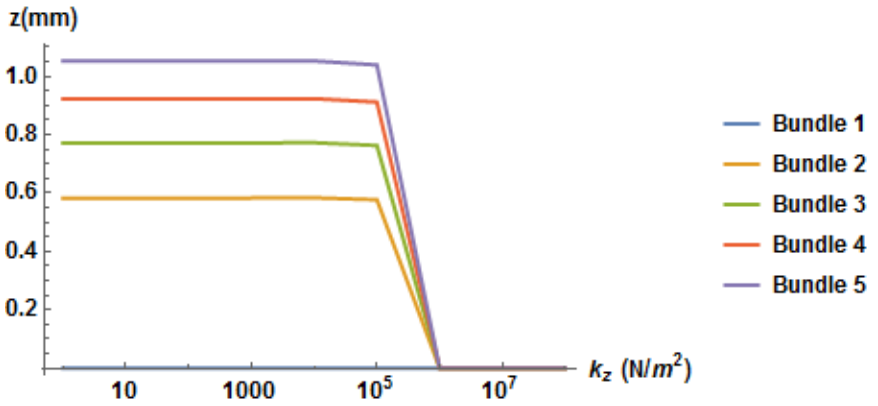

Figure 11: Effect of the foundation stiffness in the z-direction on the wrinkle formation

4. CONCLUSIONS

In this paper, a simplified model simulating the deformations of a tow steered using the AFP process. The tow is modeled as multiple bundles deforming in space and laying on a stiff foundation. The material properties of the tow in transverse and shear directions are neglected in the energy formulation when compared with the longitudinal stiffness. The resulting total energy of the system is minimized for the case of small strains and large rotations, thus generating the governing equations in the form of a system of nonlinear differential equations. A numerical solution algorithm is presented to solve the unknown functions and end-point forces in the

governing equations. The model is implemented for the case of a tow steered at a constant curvature and placed on a flat surface. Results show that at small length scale, the differential length between the tow and the path is absorbed through compressive and tensile strains. At a larger length, wrinkling and fiber bunching can occur on the compressive side of the tow, whereas tow bunching/straightening occurred on the tensile side. The effect of the stiffness of the foundation on the wrinkling formation is studied. For a weak foundation ($k < 10^5\ N/m^2$), the wrinkling magnitude is not affected when compared to no adhesion. For a larger value of the foundation's stiffness, wrinkles collapse and the differential length is absorbed through strain deformations.

Future work will include the interaction of multiple bundles in the transverse and shear directions, and thus possibly capturing the tow folding mechanism on the tensile side. In addition, experimental work is necessary to correlate the values of the stiffness of the foundation with respect to other process parameters such as surface temperature, roller pressure, and layup speed.

5. ACKNOWLEDGMENTS

The authors would like to thank The Boeing Company for their support of this work.

6. REFERENCES

1. G. Rousseau, R. Wehbe, J. Halbritter, and R. Harik, "Automated Fiber Placement Path Planning: A State-of-the-art review," *Comput. Des. Appl.*, vol. 16, no. 2, pp. 172–203, 2019. doi:10.14733/cadaps.2019.172-203.
2. A. Sabido, L. Bahamonde, R. Harik, and M. J. L. Van Tooren, "Maturity assessment of the laminate variable stiffness design process," *Compos. Struct.*, vol. 160, pp. 804–812, 2017. doi:10.1016/j.compstruct.2016.10.081.
3. R. Harik, C. Saidy, S. Williams, Z. Gurdal, and B. Grimsley, "Automated Fiber Placement Defect Identity Cards : Cause , Anticipation , Existence , Significance , and Progression," in *SAMPE Conference & Exhibition*, 2018.
4. D. H. J. A. Lukaszewicz, C. Ward, and K. D. Potter, "The engineering aspects of automated prepreg layup: History, present and future," *Compos. Part B Eng.*, vol. 43, no. 3, pp. 997–1009, 2012. doi:10.1016/j.compositesb.2011.12.003.
5. R. Wehbe, "Modeling of Tow Wrinkling in Automated Fiber Placement based on Geometrical Considerations," University of South Carolina, 2017.
6. R. Y. Wehbe, R. Harik, and Z. Gurdal, "In-plane tow deformations due to steering in automated fiber placement," in *AIAA Scitech 2019 Forum*, American Institute of Aeronautics and Astronautics, 2019. doi:10.2514/6.2019-1271.
7. S. Rajan, M. A. Sutton, R. Wehbe, B. Tatting, Z. Gürdal, and A. Kidane, "Experimental investigation of prepreg slit tape wrinkling during automated fiber placement process using StereoDIC," *Compos. Part B*, vol. 160, no. December 2018, pp. 546–557, 2019. doi:10.1016/j.compositesb.2018.12.017.

8. A. Beakou, M. Cano, J. B. Le Cam, and V. Verney, “Modelling slit tape buckling during automated prepreg manufacturing: A local approach,” *Compos. Struct.*, vol. 93, no. 10, pp. 2628–2635, 2011. doi:10.1016/j.compstruct.2011.04.030.
9. M. Y. Matveev, P. J. Schubel, A. C. Long, and I. A. Jones, “Understanding the buckling behaviour of steered tows in Automated Dry Fibre Placement (ADFP),” *Compos. Part A Appl. Sci. Manuf.*, vol. 90, pp. 451–456, 2016. doi:10.1016/j.compositesa.2016.08.014.
10. R. Wehbe, B. F. Tatting, R. Harik, Z. Gürdal, A. Halbritter, and S. Wanthal, “TOW-PATH BASED MODELING OF WRINKLING DURING THE AUTOMATED FIBER PLACEMENT PROCESS,” *Compos. Adv. Mater. Expo CAMX2017*, 2017.
11. P. M. Hormann, *Thermoset automated fibre placement - on steering effects and their prediction*. 2015.